Ultrafast structural dynamics studied by kilohertz time-resolved x-ray diffraction*

Guo Xin(郭 鑫)[a)b)], Jiang Zhou-Ya(江舟亚)[c)d)], Chen Long(陈 龙)[c)d)], Chen Li-Ming(陈黎明)[b)d)], Xin Jian-Guo(辛建国)[a)], Peter M. Rentzepis[e)], and Chen Jie(陈 洁)[c)d)†]

[a)] *School of Optoelectronics, Beijing Institute of Technology, Beijing* 100081, *China*

[b)] *Beijing National Laboratory of Condensed Matter Physics, Institute of Physics, Chinese Academy of Sciences, Beijing* 100190, *China*

[c)] *Key Laboratory for Laser Plasmas (Ministry of Education) and Department of Physics and Astronomy, Shanghai Jiao Tong University, Shanghai* 200240, *China*

[d)] *IFSA Collaborative Innovation Center, Shanghai Jiao Tong University, Shanghai* 200240, *China*

[e)] *Electrical & Computer Engineering, Texas A & M University, College Station, TX* 77843, *USA*

(Received 29 January 2015; revised manuscript received 21 May 2015; published online 20 August 2015)

Ultrashort multi-keV x-ray pulses are generated by electron plasma produced by the irradiation of femtosecond pulses on metals. These sub-picosecond x-ray pulses have extended the field of x-ray spectroscopy into the femtosecond time domain. However, pulse-to-pulse instability and long data acquisition time restrict the application of ultrashort x-ray systems operating at low repetition rates. Here we report on the performance of a femtosecond laser plasma-induced hard x-ray source that operates at 1-kHz repetition rate, and provides a flux of 2.0×10^{10} photons/s of Cu K_α radiation. Using this system for time-resolved x-ray diffraction experiments, we record in real time, the transient processes and structural changes induced by the interaction of 400-nm femtosecond pulse with the surface of a 200-nm thick Au (111) single crystal.

Keywords: ultrafast x-ray diffraction, transient structures, lattice deformation

PACS: 87.15.ht, 67.80.de, 63.70.+h **DOI:** 10.1088/1674-1056/24/10/108701

1. Introduction

Since its discovery in 1895, x-ray has played an important role in scientific research, especially in understanding the detailed structures of materials. Most of our knowledge concerning inorganic and organic crystal structures, on an atomic scale, has been obtained from x-ray diffraction data. Traditional x-ray techniques can only provide a static picture of the structure, owing to their limited time resolutions. However, with the progress in ultrafast laser technology, x-ray techniques with time resolution from picoseconds to femtoseconds also become possible. Ultrashort laser pulses have been used to generate an intense burst of coherent and incoherent energetic x-ray pulses. Ultrafast monochromatic x-ray pulses have found a wide application in the study of ultrafast structural dynamics in solid state media, such as phase transitions[1–3] and coherent phonon generation in single crystal lattices.[4,5] In addition to accelerator-generated femtosecond hard x-ray sources, such as XFEL, laser plasma-based x-ray sources developed over the past two decades have proven to be a convenient method of constructing the table-top, relatively inexpensive sub-picosecond x-ray systems, that may be used for ultrafast x-ray diffraction studies. In addition, with the generation of sub-picosecond x-ray continuum from such table-top systems, ultrafast extended x-ray absorption fine structure (EXAFS) experiments have become feasible in university laboratories.[6,7]

Ultrashort laser plasma x-ray pulses are generated by the interaction of intense femtosecond laser pulses of above 10^{15} W/cm^2, with targets such as liquids[8] and inert gases,[9,10] and mostly with metallic solids.[11,12] The design of the components of the solid target varies from rods and rotating disks to wires[4,13] and metallic thin foils. One of the main advantages of laser plasma x-ray sources is the short time width (femtosecond) of the generated x-ray pulses. These ultrashort x-ray pulses are generated by the laser plasma electrons, which are accelerated by the strong electric field of the laser pulse which impact them onto the target metal with sufficiently high energy density to ionize core electrons, thus inducing the emission of characteristic hard x-rays. The efficiency of producing characteristic x-ray lines is strongly dependent on the laser intensity[14] and the contrast between the pre-pulse and the main pulse.[15,16] Owing to the fact that the interaction time is limited by the duration of the laser pulse, the time width of the emitted x-ray pulses is estimated to be from tens to a few hundreds of femtoseconds.[17]

Most previous laser-based ultrashort x-ray sources operated in a single shot mode or at low repetition rate, up to 10 Hz, with 20 mJ–200 mJ pulse energies and 50 fs–100 fs pulse widths.[7,18] The laser pulse energies of these sources varied from pulse to pulse, which resulted in a low stability

*Project supported by the National Natural Science Foundation of China (Grant Nos. 61222509 and 11421064) and the W. M. Keck Foundation.

†Corresponding author. E-mail: jiec@sjtu.edu.cn

© 2015 Chinese Physical Society and IOP Publishing Ltd

of the x-ray flux in each pulse. Therefore, a long integration time from tens of minutes up to hours was usually necessary in order to acquire reasonable dynamic data.[19] Recently, reliable and high flux ultrashort x-ray sources have been gradually developed based on kilohertz femtosecond lasers each with a higher average power[11,20,21] and a shorter laser pulse width, which promise to become important devices for future ultrafast research and other applications. In this paper, we report an efficient ultrashort Cu K_α x-ray source built at Shanghai Jiao Tong University. It consists of a Legend Elite Duo USP Coherent table-top laser that emits 800-nm, 35-fs, 6.3-mJ pulses at 1-kHz repetition rate. In this paper we present time-resolved x-ray diffraction experiments that use this system, which allows us to study with sub-picosecond time resolution several ultrafast phenomena as well as transient structures that occur in a 200-nm thick Au (111) single crystal film.

2. Kilohertz ultrashort x-ray source

A schematic representation of our kHz ultrafast x-ray diffraction experimental system is presented in Fig. 1. The physical size of this system including the x-ray source is less than 1.5 m×1.5 m, which makes it rather easy to construct and operate at university laboratory. This experimental system consists of a commercial femtosecond laser, and a homemade x-ray chamber where sub-picosecond 8-keV x-rays are generated by the interaction of the 800-nm optical pulses with a moving thin film (30 μm) copper target. The laser output is split into two parts by an 8:2 optical beam-splitter. The 20% output is frequency-doubled, by means of a 0.2-mm thick Type I BBO crystal, to produce the 167-μJ, 35-fs, 400-nm second harmonic generation (SHG) pump pulse(s) used to initiate the transient processes. The 80% main beam pulse is expanded four times in diameter, and focuses onto the moving copper foil target by a 90° off-axis parabolic (OAP) mirror with an effective focal length of 127 mm. The root-mean-square deviation of the pulse energy is measured to be within 0.5%, which is one of the prerequisites for a stable ultrafast x-ray source. The laser pulse, with a full width at half maximum (FWHM) diameter of ∼10 μm and a peak laser intensity of 1.8×10^{17} W/cm^2, strikes the metal target that consists of a 25-μm thick and 20-mm wide fresh moving copper strip to generate the hot electron plasma. Fast electrons are also produced during the formation of the laser plasma, and their average energy is estimated to be on the order of a few tens of keV.[22,23] The resulting sub-picosecond Cu K_α x-ray pulses serve as the probe pulses for the detection and measurement of ultrafast structural dynamics in real time. The 75-m long strip of the copper foil connected to two coils is placed inside the x-ray source vacuum chamber at a base pressure of 10^{-3}-Torr (1 Torr = 1.33322×10^2 Pa), which is sufficiently low to eliminate energy loss due to air ionization. The moving speed of the Cu strip is chosen so that each laser pulse irradiates a fresh copper surface. When the copper strip segment is near its end, the chamber is raised up by 1-mm and the rotation direction of the coils remains unchanged. Both the 3-mm sapphire optical entrance window and the 250-beryllium x-ray exit window would be polluted by the foil emitted debris if not protected. We used a 20-μm thick and 40-mm wide Mylar tape to protect both windows, because it is highly transparent to both the 800-nm optical beam and Cu K_α and K_β x-ray radiations at 8.04 keV and 8.91 keV, respectively. The Mylar tape is placed between the copper film and the two windows, which continuously move to protect the optical and x-ray windows during each experiment. This design is utilized in other kilohertz systems.[24] Our design can significantly reduce the size of the vacuum chamber and its complexity. The ultrashort x-ray output is measured with an Si p-intrinsic-n (PIN) x-ray photon detector (Amptek, X-123), which is equipped with a 500-μm thick, 6-mm^2 area silicon chip with an approximately 100% detection efficiency for 8-keV x-rays. The detector is sealed with a 100-μm thick beryllium window through which 8-keV x-ray photons propagate with negligible loss. The detector was placed 500-mm away from the optical focal spot, and the x-ray output travels 30 mm through the vacuum and 470 mm in air, which results in 59% attenuation in the transmission of Cu K_α x-ray photons. A 500-μm diameter lead aperture and a 200-μm thick aluminum filter are placed in front of the detector to ensure its operation under the single-photon counting condition.

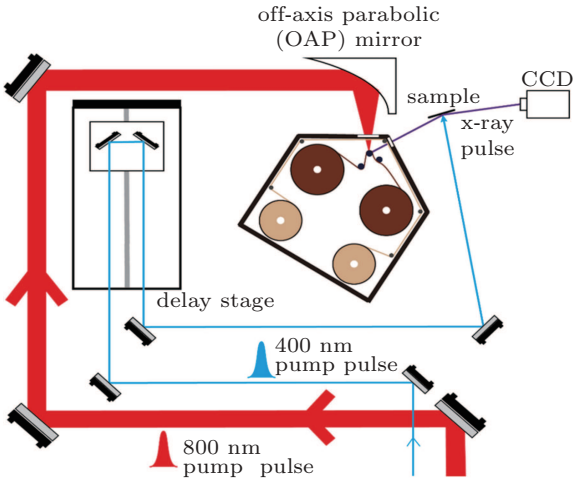


Fig. 1. (color online) Top view of experimental configuration.

The corresponding x-ray spectrum obtained is shown in Fig. 2, which consists of both bremsstrahlung continuum and Cu characteristic radiations. Assuming an isotropic production of Cu K_α radiation in a solid angle of 4π and taking the detection efficiency into consideration, we calculate the photon flux to be 2.0×10^{10} photons/s with 5.1×10^6 conversion efficiency from 800-nm photons to Cu K_α. Although Cu

$K_{\alpha 1}$ and $K_{\alpha 2}$ characteristic lines are not resolved due to the ~120-eV energy resolution of the Si-PIN detector, they could be clearly distinguished by both a 500-nm GaN [0001] crystal and its 500-μm Si (111) substrate located at 115 mm from the x-ray source. The inset in Fig. 2 shows a high-resolution separation of the two Cu K_α lines by the GaN [0001] crystal spectrometer, which are captured by a 1340 × 1300 x-ray charge-coupled device (CCD) camera (PIXIS-XB:1300R, Princeton Instruments) placed 122-mm away from the GaN crystal. Under the above configuration, the line width of Cu $K_{\alpha 1}$ is 13.86 eV, resolved by the 500-μm Si (111) crystal, suggesting that the diameter of x-ray source is not more than 55 μm.[25] The larger than the 10-μm laser focal spot size of x-ray source is mainly due to the long term instability of the laser beam and the vibration of the copper tape.

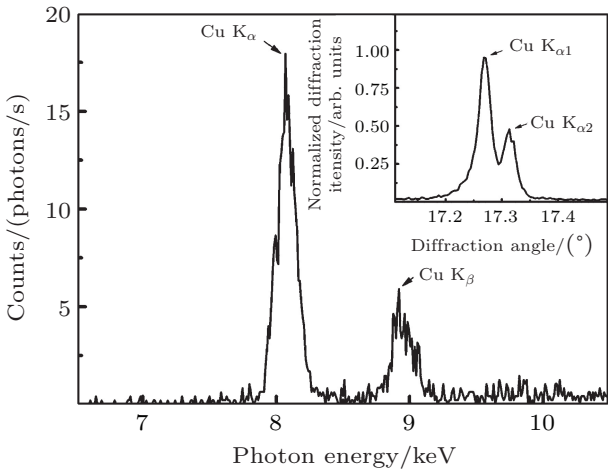


Fig. 2. Spectrum of Cu K_α and K_β radiation obtained at 1-kHz repetition rate. Inset: Spectrally resolved Cu $K_{\alpha 1}$ and $K_{\alpha 2}$ fine structure components of the x-ray radiation by a 500-nm GaN [0001] crystal.

We also measure the total x-ray generation as a function of target position, ΔX, with respect to the best focal spot, where the OAP effective focal point is right on the target as shown in Fig. 3. We observe a maximum output in each direction off the location of the best focal spot. The slightly low x-ray yield at the best focal spot agrees with previously published data.[26] This is qualitatively explained as the re-absorption of the x-ray photons produced inside the target at this position. At the best focal spot, the higher laser intensity leads to high energy electrons; therefore, they penetrate into the target more deeply, most of which are re-absorbed. Consequently, the x-ray radiation emitted drops at the best focal spot. It should be noted that the distance between two maxima, in spite of the different focal lengths of different OAP mirrors, applied to our and other systems,[26] is measured to be around 0.4 Rayleigh length (RL) of the mirror. In our case, the distance, about 0.1 mm, is much larger than the 25-μm thickness of the target copper film, which allows for only 40-μm tolerance.

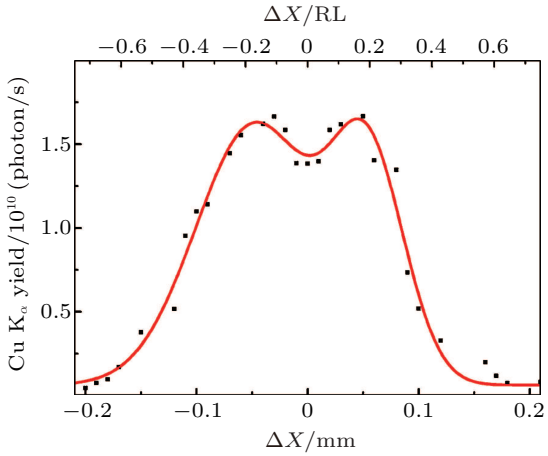


Fig. 3. (color online) Total amount of Cu K_α emission as a function of target displacement from the best focal spot. Positive values of the distance indicate that the focus is situated in front of the target. For negative values the focus is within the target.

3. Ultrafast x-ray diffraction

Using our kHz repetition rate, sub-picosecond x-ray experimental system described in the previous section, we first study the transient processes induced by 1-kHz, 35-fs, 400-nm SHG pulses impinging on the surface of a 200-nm thick Au (111) single crystal film grown on mica substrate. The basic experimental concept of ultrafast time-resolved measurements, based on the pump–probe technique, has well been established in the optical area since the 1960s.[27] Such a real-time method is easily extended to the x-ray regime by using an optical pump pulse for excitation and a synchronized ultrashort x-ray pulse to act as the probe pulse, which monitors the transient structural changes induced by the interaction of the pump pulse with the sample. In this optical pump x-ray probe experiment, we use the SHG at 400 nm for excitation which has a penetration length of 17 nm that fits well with the interband absorption of gold. The change in the Au (111) structure as a function of time is probed with 8.04-keV Cu K_α x-ray pulses. Synchronization between the optical pump and x-ray pulse is achieved by making the 400-nm pump pulse propagate through a delay line that could be adjusted within a resolution of 2 μm, which corresponds to a time interval of 6 fs.

After the optical pulse irradiates into the surface layer of the crystal, the surface electrons absorb the laser energy and the electron gas temperature increases to thousands of degrees. Because the heat capacity of electrons is about two orders of magnitude smaller than that of the lattice, the electron temperature can be very high for a short time period while the lattice remains cold. As a result, the temperature distribution along the crystal thickness becomes non-uniform, which causes a distortion in lattice spacing.[28] Because the diffraction of x-ray radiation is determined by the Bragg's law: $n\lambda = 2d\sin\theta$ (n is an integer), even small changes in the inter-atomic spacing d of a crystal result in a shift in the diffraction angle θ. The

Bragg diffraction angle of Au (111) is 19.1° for Cu K_α radiation. The relationship between the angle shift $\Delta\theta$ and the lattice spacing change Δd is given by $\Delta d/d = -\Delta\theta/\tan\theta$. These x-ray diffraction changes are recorded by the x-ray CCD camera located 150 mm from the crystal. The camera is cooled to −60 °C and protected by a 250-μm thick beryllium window from visible and ultraviolet (UV) light. The size of the incident x-ray pulse is limited by a 0.25-mm wide tungsten slit to a divergence of a few milli-radian, and the x-ray beam impinging on the crystal could be blocked by a 1-mm wide aluminum strip moving in the horizontal direction along the surface. The size of the x-ray beam in the vertical direction is larger than the 10-mm height of the crystal and much larger than the 2-mm spot on the crystal formed by the pump laser pulse. Therefore, we could record simultaneously the diffraction signals from both the 400-nm irradiated area and non-irradiated area of the crystal. The diffracted signal from the 200-nm Au (111) crystal shown in the inset of Fig. 4 is obtained with the x-ray CCD after 20-s exposure. The experimental rocking curves from both the irradiated and non-irradiated areas of the Au (111) crystal at +50-ps delay time are presented in Fig. 4. A positive delay means that the pump laser pulse is leading the probe x-ray pulse. Each x-ray rocking curve is fitted with a single Gaussian function. The shift of the rocking curve is defined as the moving of the fitted peak center, where a shift toward smaller diffraction angles indicates lattice expansion. A slight broadening of the x-ray rocking curve is observed at positive delay time, measured by the FWHM change of the fitted rocking curve, compared with the rocking curve of the non-pump areas (solid curves).

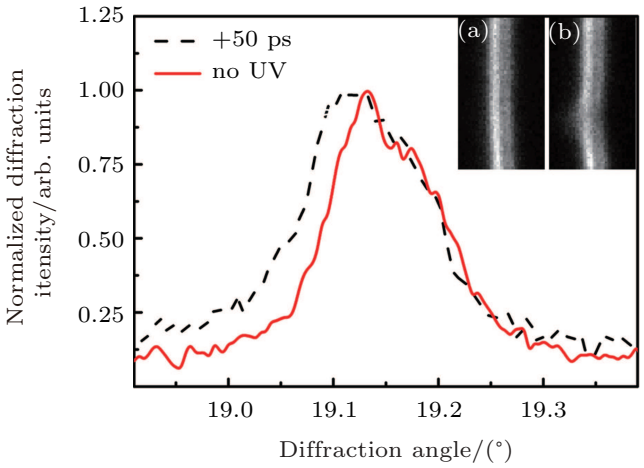


Fig. 4. (color online) Rocking curves of the heated and cold areas of a 200-nm Au (111) crystal, at 50-ps delay time. Inset: CCD images recorded after 20-s exposure: (a) without 400-nm and (b) with 400-nm illumination.

As discussed previously, a large temperature gradient could be generated upon femtosecond laser excitation of the gold sample surface. Such a temperature gradient induces a further pressure wave, the "blast wave",[18,29,30] which lasts a very short time, 1 ps–2 ps and propagates with sound velocity (c_s) through the crystal, inducing strain in its path. After 2 ps, the heated gold lattice starts to relax and expand, and the strain pulse, which consists mostly of longitudinal acoustic phonons, propagates through the bulk of the Au (111) crystal. The propagation of the acoustic waves through the bulk of the crystal causes expansion and contraction in lattice structure, which is recorded in real time and with sub-picosecond resolution, by our time-resolved x-ray experimental system. The peak of the rocking curve is found to shift towards smaller diffraction angles as a function of delay time in Fig. 5. These data show that the lattice constant increases as the lattice expands, reaching a maximum at 46 ps after excitation. The characteristic time of an acoustic wave is given by the time that it takes to travel inside the crystal with a thickness d as a standing wave, i.e., $\tau_{ac} = 2d/c_s$. For $d = (200 \pm 0.6)$ nm and $c_s = 3.24$ km/s along the Au (111) direction, $\tau_{ac} = (123 \pm 0.4)$ ps. The 123 ps, characteristic time, measured in our experiments, is in very good agreement with the observed experimental periodicity of the Bragg peak shift, (124 ± 4) ps, which is an indication of the lattice breathing motion along the surface normal.

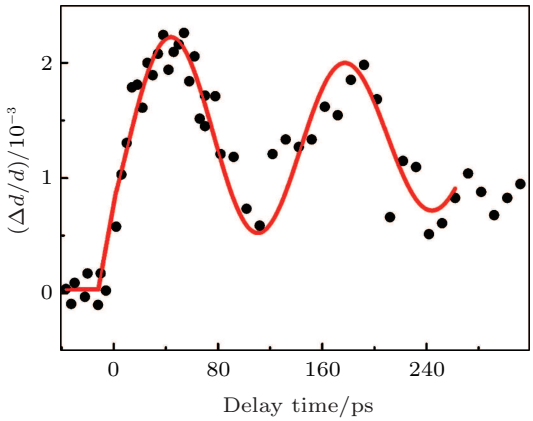


Fig. 5. (color online) Variation of lattice constant of a 200-nm Au (111) crystal with pump–probe time delay.

It should be noted that each rocking curve (see the inset in Fig. 4) is obtained by the 1-kHz ultrafast x-ray system in a 20-s exposure. These experimental results are similar to those obtained by a 10-Hz system with 30 min–60 min exposure for each datum point. The almost two-order reduction in data acquisition time suggests that such a system could be successfully applied to the study of the ultrafast dynamics of structures, such as ferroelectric/ferromagnetic superlattices and few-layer two-dimensional materials, exhibiting relatively low x-ray diffraction efficiency. In addition, this kHz experimental system may be utilized in the studies of sub-picosecond x-ray powder diffraction.

4. Conclusions

In this paper, we describe the design, construction, and performance of our novel reflective mode ultrafast, 1-kHz

high repetition rate, laser plasma-based, multi-keV hard x-ray source. This system generates Cu K_α 8.04-keV x-ray pulses, with a flux of 2.0×10^{10} photons/s. We utilize this new ultrafast x-ray experimental system to measure, with sub-picosecond resolution, the changes in the structure and other transient phenomena, such as the shift and broadening of the rocking curves that occur in an Au (111) thin crystal after 50-fs 400-nm pulse excitation. We also show that these time-resolved x-ray techniques record accurately, with sub-picosecond resolution, ultrafast structural changes and dynamics of lattice distortions by means of synchronized femtosecond optical pump pulses and sub-picosecond, multi-keV x-ray robe pulses. After further improvement in stability and an increase in x-ray photon flux per pulse, we expect our system to be able to measure in the near future transient processes and structures that occur in the femtosecond-to-picosecond range.

Acknowledgment

We thank Mr. Zhu Peng-Fei and Mr. Zhao Xin-Ri for mechanical design and Mr. Tan Ye-Teng for technical support, and Mr. Li Run-Ze for valuable discussion.

References

[1] Rousse A, Rischel C, Fourmaux S, Uschmann I, Sebban S, Grillon G, Balcou P, Förster E, Geindre J P and Audebert P 2001 *Nature* **410** 65
[2] Sokolowski-Tinten K, Blome C, Dietrich C, Tarasevitch A, Von Hoegen M H, von der Linde D, Cavalleri A, Squier J and Kammler M 2001 *Phys. Rev. Lett.* **87** 225701
[3] Chen X C, Zhou J P, Wang H Y, Xu P S and Pan G Q 2011 *Chin. Phys. B* **20** 096102
[4] Sokolowski-Tinten K, Blome C, Blums J, Cavalleri A, Dietrich C, Tarasevitch A, Uschmann I, Förster E, Kammler M and Horn-von-Hoegen M 2003 *Nature* **422** 287
[5] Bargheer M, Zhavoronkov N, Gritsai Y, Woo J, Kim D, Wörner M and Elsässer T 2004 *Science* **306** 1771
[6] Silies M, Witte H, Linden S, Kutzner J, Uschmann I, Forster E and Zacharias H 2009 *Appl. Phys. A* **96** 59
[7] Tomov I, Chen J, Ding X and Rentzepis P 2004 *Chem. Phys. Lett.* **389** 363
[8] Reich C, Laperle C M, Li X, Ahr B, Benesch F and Rose-Petruck C G 2007 *Opt. Lett.* **32** 427
[9] Döppner T, Fennel T, Diederich T, Tiggesbäumker J and Meiwes-Broer K 2005 *Phys. Rev. Lett.* **94** 013401
[10] Chen L, Liu F, Wang W, Kando M, Mao J, Zhang L, Ma J, Li Y, Bulanov S and Tajima T 2010 *Phys. Rev. Lett.* **104** 215004
[11] Hagedorn M, Kutzner J, Tsilimis G and Zacharias H 2003 *Appl. Phys. B* **77** 49
[12] Hou B, Nees J, Mordovanakis A, Wilcox M, Mourou G, Chen L, Kieffer J C, Chamberlain C and Krol A 2006 *Appl. Phys. B* **83** 81
[13] Rose-Petruck C, Jimenez R, Guo T, Cavalleri A, Siders C W, Rksi F, Squier J A, Walker B C, Wilson K R and Barty C P 1999 *Nature* **398** 310
[14] Schlegel T, Bastiani S, Gremillet L, Geindre J P, Audebert P, Gauthier J C, Lefebvre E, Bonnaud G and Delettrez J 1999 *Phys. Rev. E* **60** 2209
[15] Chen L, Kando M, Xu M, Li Y, Koga J, Chen M, Xu H, Yuan X, Dong Q and Sheng Z 2008 *Phys. Rev. Lett.* **100** 045004
[16] Sheng Z M, Wen S M, Yu L L, Wang W M, Cui Y Q, Chen M and Zhang J 2015 *Chin. Phys. B* **24** 015201
[17] Reich C, Uschmann I, Ewald F, Düsterer S, Lübcke A, Schwoerer H, Sauerbrey R, Förster E and Gibbon P 2003 *Phys. Rev. E* **68** 056408
[18] Chen J, Chen W K and Rentzepis P M 2011 *J. Appl. Phys.* **109** 113522
[19] Chen J, Tomov I, Elsayed-Ali H and Rentzepis P 2006 *Chem. Phys. Lett.* **419** 374
[20] Hou B, Easter J, Mordovanakis A, Krushelnick K and Nees J A 2008 *Opt. Express* **16** 17695
[21] Huang K, Li M, Yan W, Guo X, Li D, Chen Y, Ma Y, Zhao J, Li Y and Zhang J 2014 *Rev. Sci. Instrum.* **85** 113304
[22] Gibbon P and Förster E 1996 *Plasma Phys. Control. Fusion* **38** 769
[23] Malka V, Faure J, Gauduel Y A, Lefebvre E, Rousse A and Phuoc K T 2008 *Nat. Phys.* **4** 447
[24] Zamponi F, Ansari Z, Schmising C V K, Rothhardt P, Zhavoronkov N, Woerner M, Elsaesser T, Bargheer M, Trobitzsch-Ryll T and Haschke M 2009 *Appl. Phys. A* **96** 51
[25] Oulianov D A, Tomov I V, Lin S H and Rentzepis P M 2001 *J. Chin. Chem. Soc.* **48** 127
[26] Eder D, Pretzler G, Fill E, Eidmann K and Saemann A 2000 *Appl. Phys. B* **70** 211
[27] Norrish R and Porter G 1949 *Nature* **164** 658
[28] Okada Y and Tokumaru Y 1984 *J. Appl. Phys.* **56** 314
[29] Hohlfeld J, Wellershoff S S, Güdde J, Conrad U, Jähnke V and Matthias E 2000 *Chem. Phys.* **251** 237
[30] Gan Y and Chen J 2010 *Mech. Mater.* **42** 491